THE JOURNAL OF BIOLOGICAL CHEMISTRY
Vol. 276, No. 50, Issue of December 14, pp. 47474–47482, 2001
Printed in U.S.A.

Mechanism of Product Chain Length Determination and the Role of a Flexible Loop in *Escherichia coli* Undecaprenyl-pyrophosphate Synthase Catalysis*

Received for publication, July 18, 2001, and in revised form, September 20, 2001
Published, JBC Papers in Press, October 1, 2001, DOI 10.1074/jbc.M106747200

Tzu-Ping Ko‡§, Yi-Kai Chen‡§, Howard Robinson¶, Pei-Chun Tsai‡, Yi-Gui Gao¶, Annie P.-C. Chen‖, Andrew H.-J. Wang‡‖, and Po-Huang Liang‡‖‡‡**

From the ‡Institute of Biological Chemistry, Academia Sinica, Taipei 115 and ‖Institute of Biochemical Sciences, National Taiwan University, Taipei 106, Taiwan

The *Escherichia coli* undecaprayl-pyrophosphate synthase (UPPs) structure has been solved using the single wavelength anomalous diffraction method. The putative substrate-binding site is located near the end of the βA-strand with Asp-26 playing a critical catalytic role. In both subunits, an elongated hydrophobic tunnel is found, surrounded by four β-strands (βA-βB-βD-βC) and two helices (α2 and α3) and lined at the bottom with large residues Ile-62, Leu-137, Val-105, and His-103. The product distributions formed by the use of the I62A, V105A, and H103A mutants are similar to those observed for wild-type UPPs. Catalysis by the L137A UPPs, on the other hand, results in predominantly the formation of the C_{70} polymer rather than the C_{55} polymer. Ala-69 and Ala-143 are located near the top of the tunnel. In contrast to the A143V reaction, the C_{30} intermediate is formed to a greater extent and is longer lived in the process catalyzed by the A69L mutant. These findings suggest that the small side chain of Ala-69 is required for rapid elongation to the C_{55} product, whereas the large hydrophobic side chain of Leu-137 is required to limit the elongation to the C_{55} product. The roles of residues located on a flexible loop were investigated. The S71A, N74A, or R77A mutants displayed 25–200-fold decrease in k_{cat} values. W75A showed an 8-fold increase of the FPP K_m value, and 22–33-fold increases in the IPP K_m values were observed for E81A and S71A. The loop may function to bridge the interaction of IPP with FPP, needed to initiate the condensation reaction and serve as a hinge to control the substrate binding and product release.

Prenyltransferases catalyze consecutive condensation reactions of isopentenyl pyrophosphate (IPP)[1] with allylic pyrophosphate to generate linear isoprenyl polymers. The isoprenylates undergo further modification to form a variety of isoprenoid structures including steroids, terpenes, the side chains of respiratory quinones, carotenoids, natural rubber, the glycosyl carrier lipid, and prenyl proteins (1, 2). *E*- and *Z*-type prenyltransferases synthesize *trans* and *cis* double bonds, respectively, through the condensation reactions of IPP (3). Each of the *E*-type enzymes catalyzes the formation of a product having a specific chain length ranging from C_{10} to C_{50} (4).

Two conserved DD*XX*D motifs are observed in *E*-type enzymes (5–7). X-ray structural (8) and site-directed mutagenesis studies (9–12) of farnesyl-pyrophosphate synthase (FPPs) have shown that the first aspartate-rich motif binds the allylic substrate, whereas the second DD*XX*D binds IPP via Mg^{2+}. Mutagenesis studies indicate that the 5th amino acid residue (Phe-77) upstream from the first DD*XX*D plays a critical role in controlling the chain length of the final product formed in the reaction catalyzed by *E*-type geranylgeranyl-pyrophosphate synthase from archaebacterium (13). By substituting this large residue with the smaller Ser, product synthesis was shifted from the production of C_{20} product to C_{25} and C_{30} products (14). Double (F77G/L74G) and triple (F77G/L74G/I71G) mutants were observed to catalyze the formation of even longer chain products (15). Replacing the active site aromatic residues Phe-112 and Phe-113 with smaller amino acids produced FPPs mutants that synthesize C_{20} geranyl pyrophosphate (F112A), C_{25} geranylfarnesyl pyrophosphate (F113S), and longer products (F112A/F113S) (16). Analysis of the F112A/F113S structure shows that it contains an enlarged active site that is possibly related to increased product size.

On the other hand, *Z*-type isoprenyl-pyrophosphate synthases such as undecaprenyl-pyrophosphate synthase (UPPs) and dehydrodolichyl-pyrophosphate synthase catalyze the formation of long chain products ranging from C_{55} to C_{100} (17, 18). UPPs, the subject of this paper, generates a C_{55} product by catalyzing the chain elongation of farnesyl pyrophosphate (FPP) via sequential condensation reactions of eight IPP, which serves as a carrier in transporting lipid II across the membrane in bacterial cell wall biosynthesis (19, 20). Despite close similarities in the chemistry catalyzed, no sequence homology exists between *Z*-type and *E*-type enzymes (21, 22). To understand better the *Z*-type enzyme catalysis, we have studied the reaction mechanism and kinetics of *Escherichia coli* UPPs (23),

* This work was supported in part by grants from Academia Sinica (to A. H. J. W. and P. H. L.), by Grant GM41612 from the National Institutes of Health (to A. H. J. W.), and by Grant NSC89-2113-M-001-061 from the Taiwan National Science Council (to P. H. L.). The costs of publication of this article were defrayed in part by the payment of page charges. This article must therefore be hereby marked "*advertisement*" in accordance with 18 U.S.C. Section 1734 solely to indicate this fact.

The atomic coordinates and structure factors (code 1JP3) have been deposited in the Protein Data Bank, Research Collaboratory for Structural Bioinformatics, Rutgers University, New Brunswick, NJ (http://www.rcsb.org/).

§ Both authors contributed equally to this work.

¶ Present address: Dept. of Biochemistry, School of Molecular and Cellular Biology, University of Illinois at Urbana-Champaign, Urbana, IL 61801.

** To whom correspondence may be addressed. Tel.: 886-2-2788-1981; Fax: 886-2-2788-9759; E-mail: ahjwang@gate.sinica.edu.tw.

‡‡ To whom correspondence may be addressed. Tel.: 886-2-2785-5696 (ext. 6070); Fax: 886-2-2788-9759; E-mail: phliang@gate.sinica.edu.tw.

[1] The abbreviations used are: IPP, isopentenyl pyrophosphate; FPPs, farnesyl-pyrophosphate synthase; FPP, farnesyl pyrophosphate; UPPs, undecaprenyl-pyrophosphate synthase; UPP, undecaprenyl pyrophosphate; NiNTA, nickel-nitrilotriacetic acid; PEG, polyethylene glycol; r.m.s.d., root mean square deviation; PCR, polymerase chain reaction.

TABLE I
Data collection and refinement statistics of the E. coli UPPs crystal

Space group	$P2_12_12_1$	
Unit cell dimension (Å)	a = 64.18; b = 67.33; c = 110.15	
Resolution range (Å)	20–1.80	1.86–1.80
Total number of reflections[a]	44,770	4420
$\langle I/\sigma(I)\rangle$	25.7	6.5
R_{merge} (%)	6.8	35.6
Completeness (%)	99.6	99.9
Number of reflections >0 $\sigma(F)$[b]	44,367	4313
R_{work} for 95% working data set	0.194	0.236
R_{free} for 5% test data set	0.228	0.247
Estimated coordinate errors (Å) using	R_{work}	R_{free}
by Luzzati plot	0.20	0.24
by SigmaA plot	0.11	0.12
Deviation from ideal stereochemistry		
r.m.s.d. bond (Å)	0.012	
Angle (°)	1.5	
Dihedral (°)	22	
Improper (°)	0.95	
Ramachandran plot (excluding prolines and glycines)		
Residues in most favored regions	358 (95%)	
Residues in additional allowed regions	19 (5%)	
Average B factor for all 4040 atoms (Å^2)	29.1	

[a] Data collected at the inflection point (λ = 0.9791 Å) of the selenium absorption edge.
[b] Prior to use in refinement, 40277 Friedel pairs of reflections were averaged with an overall R-value of 5.7%.

and we show that some aspartate and glutamate residues may play a structural and catalytic role and that their mutations affect the enzyme activity and/or substrate binding (24). Recently, the three-dimensional structure of UPPs from *Micrococcus luteus* was solved by Fujihashi *et al.* (25), and it is completely different from those of *E*-type prenyltransferases. We report the structure of *E. coli* UPPs, which is similar to the structure of *M. luteus* UPPs except that two protein conformers were discovered for *E. coli* UPPs. The large amino acid residues Ile-62, Leu-137, Val-105, and His-103, occupying the bottom portion of an elongated hydrophobic tunnel from the structure of *E. coli* UPPs were replaced with Ala using site-directed mutagenesis to study the mechanism of product chain length determination. In addition, two amino acid residues, Ala-69 and Ala-143, located near the top of the hydrophobic tunnel in *E. coli* UPPs, were substituted with Leu and Val, respectively, as seen in the *Mycobacterium tuberculosis Z*-type short chain FPPs (26) to examine the possible formation of a short chain product. Furthermore, a flexible loop without observable electron densities of residues 72–83 was found in both UPPs structures. Mutagenesis studies of the *M. luteus* enzyme suggest that loop residues Asn-77 and Trp-78 are important for catalysis and FPP binding (27). To address the role of this loop in *E. coli* UPPs, we generated the loop mutants S71A, E73A, N74A, W75A, R77A, and E81A and measured the impact of loop residue replacement on substrate binding and catalysis.

EXPERIMENTAL PROCEDURES

Materials—Radiolabeled [^{14}C]IPP (55 mCi/mmol) was purchased from Amersham Pharmacia Biotech, and FPP was obtained from Sigma. Reversed-phase thin layer chromatography (TLC) plates were purchased from Merck. *Taq* DNA polymerase was obtained from Life Technologies, Inc. The plasmid mini-prep kit, DNA gel extraction kit, and NiNTA resin were purchased from Qiagen. Potato acid phosphatase (2 units/mg) was purchased from Roche Molecular Biochemicals. FXa and the protein expression kit (including the pET32Xa/LIC vector and competent JM109 and BL21 cells) were obtained from Novagen. The B834 (DE3) competent cells for the production of seleno-Met UPPs was also from Novagen. Seleno-DL-methionine was purchased from Sigma. All commercial buffers and reagents were of the highest grade.

Site-directed Mutagenesis of UPPs—UPPs mutants were prepared by using PCR techniques in conjunction with the *E. coli Bos-12* UPPs gene template in the pET32Xa/Lic vector (23). The mutagenic primers used were prepared by MDBio Inc. The mutagenic oligonucleotides for performing site-directed mutagenesis are as follows: 5′-AACGGTGCTGAGGCGTTA-3′ for I62A; 5′-CTGCACCGAGCTAACGTG-3′ for H103A; 5′-CATAACGCGCGTCTGCGT-3′ for V105A, 5′-ACCGGTGCGACGCTGAAT-3′ for L137A; 5′-ACGCTGTATCTCTTTAGT-3′ for A69L; 5′-ATTGCGCTGAACTACGGT-3′ for A143V, 5′-GCCTTTGCTAGTGAAAAC-3′ for S71A; 5′-AGTGAAGCCTGGAACCGA-3′ for N74A; 5′-GAAAACGCGAACCGACCA-3′ for W75A; 5′-AACTGGAACGCACCAGCG-3′ for R77A; and 5′-CCAGCGCAGGCAGTCAGT-3′ for E81A. Subsequently, the forward primer 5′-GGTATTGAGGGTCGCATGTTGTCTGCT-3′ and reverse primer 5′-AGAGGAGAGTTAGAGCCATCAGGCTGT-3′ were used in combination with the PCR products obtained using the above mutagenic oligonucleotides to create the full-length mutant UPPs genes. The FXa cleavage site (IEGR) and the complementary sequences to the sticky ends of the linear vector pET-32Xa/LIC were included in these primers. Thirty cycles of PCR were performed using a thermocycler (Applied Biosystems) with the melting temperature at 95 °C for 2 min, annealing temperature at 42 °C for 2 min, and polymerization temperature at 68 °C for 40 s. The PCR product was subjected to electrophoresis on 0.8% agarose gel in TAE buffer, and then the gel was stained with ethidium bromide. The part of the gel containing the band of the correct size was excised, and the DNA was recovered using a DNA elution kit. The constructed gene of a mutant enzyme was ligated to the vector by incubation for 1 h at 22 °C. The recombinant UPPs plasmid was then used to transform *E. coli* JM109 competent cells that were streaked on a Luria-Bertani (LB) agar plate containing 100 μg/ml ampicillin. Ampicillin-resistant colonies were selected from the agar plate and grown in 5 ml of LB culture containing 100 μg/ml ampicillin overnight at 37 °C. The mutation was confirmed by sequencing the entire UPPs mutant gene of the plasmid obtained from the overnight culture. The correct construct was subsequently transformed to *E. coli* BL21 for protein expression. The 5-ml overnight culture of a single transformant was used to inoculate 500 ml of fresh LB medium containing 100 μg/ml ampicillin. The cells were grown to A_{600} = 0.6 and induced with 1 mM isopropyl-β-thiogalactopyranoside. After 4–5 h, the cells were harvested by centrifugation at 7,000 × g for 15 min.

Enzyme Purification—Approximately 3 g of cell paste, collected from LB broth of *E. coli* expressing mutant UPPs by centrifugation, was suspended in 25 ml of lysis buffer containing 25 mM Tris-HCl, pH 7.5,

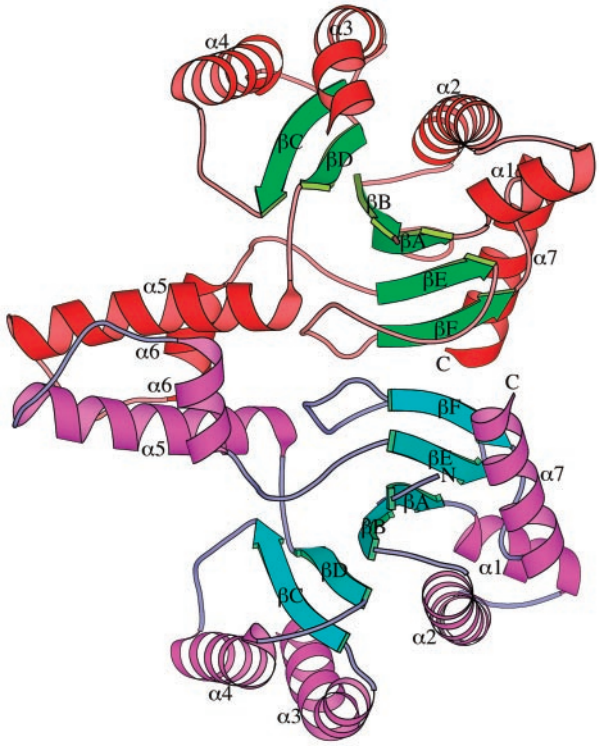

FIG. 1. **A ribbon representation of the UPPs dimer with the dyad lying horizontal.** The 7 α-helices and 6 β-strands are shown in *red* and *green* for subunit A and in *magenta* and *cyan* for subunit B. The figure was prepared using MolScript (38).

and 150 mM NaCl at 4 °C. The cell lysate, prepared with a French® pressure cell press (AIM-AMINCO spectronic Instruments), was centrifuged at 10,000 × *g* to remove cell debris. The cell-free extract was loaded onto a NiNTA column, which had been previously equilibrated with lysis buffer containing 5 mM imidazole. After exhaustive washing with this same buffer at 4 °C, the imidazole concentration of the washing buffer was increased to 30 mM. The protein-containing fractions eluted by 300 mM imidazole were dialyzed against a buffer containing 25 mM Tris-HCl, pH 7.5, and 150 mM NaCl and then subjected to FXa digestion to remove the His tag. The mixture was passed through a NiNTA column for purification. SDS-polyacrylamide gel electrophoresis analysis was performed to demonstrate the purity of UPPs mutants.

Preparation of Seleno-Met Modified UPPs—To produce seleno-Met modified UPPs, the plasmid containing UPPs gene was transformed into B834 (DE3)-competent cell. The single transformant was first grown overnight at 37 °C in LB containing 100 μg/ml ampicillin. The cells were then used to inoculate 2 liters of LeMaster Medium (28) with the supplement of 50 mg/liter seleno-DL-methionine. Isopropyl-β-D-thiogalactopyranoside was added to a final concentration of 0.75 mM for induction after the cell density reached A_{600} = 0.4. The cells were grown for another 10 h at 37 °C and then harvested by centrifugation. The subsequent purification procedure for seleno-Met UPPs was the same as for UPPs. The NiNTA-purified seleno-Met UPPs was in buffer containing 25 mM Tris-HCl, pH 7.5, and 150 mM NaCl. Triton X-100 was added into protein solution to 0.1%, and the protein was concentrated to ~5 mg/ml.

Crystallographic Analysis—UPPs was crystallized using the hanging drop set-up from Hampton Research (Laguna Niguel, CA) by mixing 2 μl of the UPPs solution (5 mg/ml in 0.1% Triton X-100) with 2 μl of the mother liquor (25% PEG400 in 100 mM sodium cacodylate, pH 5.5), equilibrating with 500 μl of the mother liquor. Crystallization of the seleno-Met enzyme was achieved under a slightly different condition by mixing 2 μl of the UPPs solution (5 mg/ml in 0.1% Triton X-100) with 2 μl of the mother liquor (10% PEG8000, 8% ethylene glycol, in 100 mM KOH-Hepes, pH 7.5), equilibrating with 500 μl of the mother liquor. In both cases, long rods of crystals appeared in 1 week.

Diffraction data were collected at the National Synchrotron Light Source beamline X4A (Brookhaven National Laboratory) at four wavelengths (low remote, inflection point, peak, and high remote) at and near the selenium absorption edge. We attempted to determine the phases using data from all four wavelengths. However, the resulting MAD-phasing electron density map could not be interpreted. Subsequently, phases were determined with the program suite SOLVE (29; also at website www.solve.lanl.gov) in the single wavelength anomalous diffraction mode, using only the inflection wavelength data in the resolution range of 20 to 1.8 Å. Six selenium sites (of 10) were found. Density modification with RESOLVE (30) yielded an overall figure of merit of 0.53 (with figure of merit = 0.86 in the 20 to 3.0-Å range).

The single wavelength anomalous diffraction-phased electron density map was of good quality at 1.8-Å resolution, allowing the polypeptide chain to be traced automatically with ARP/WARP of CCP4 (31, 32). The map clearly revealed that the dimeric structure of UPPs is the asymmetric unit.

The model was further modified manually using O (33) and refined by a crystallography and NMR system (34). Selenium atoms were used for the selenium-Met residues in the refinement. During refinement, we noticed that the enzyme structure contains a hydrophobic tunnel in which a 12-atom piece moiety of either the Triton X-100 molecule or the PEG8000 is visible in subunit A. The final model contains residues 13–71 and 86–240 in subunit A, residues 17–71 and 83–238 in subunit B, 645 water molecules, and one 12-atom piece of the PEG moiety. In the final model, all located residues have their ϕ/ψ angles in the allowable regions, and all their side chains were located. The crystal and refinement data are listed in Table I.

Measurements of K_m and k_{cat} Values for Mutant UPPs—For the measurements of kinetic parameters, mutant UPPs (0.1 μM S71A, N74A, and R77A and 0.01 μM E81A and W75A) was utilized to initiate the reaction of FPP and [^{14}C]IPP in 200-μl solutions. For IPP K_m and k_{cat} determinations, 10 μM FPP was utilized to saturate the enzyme, and IPP concentrations of 0.5-5 K_m were employed. For FPP K_m measurements, 0.2–10 μM FPP were used along with 20 μM [^{14}C]IPP. All reactions were carried out in 100 mM KOH-Hepes buffer, pH 7.5, 50 mM KCl, and 0.5 mM $MgCl_2$ at 25 °C in the presence of 0.1% Triton X-100. To measure the initial rate, 40-μl portions of the reaction mixture were periodically withdrawn within 10% substrate depletion and mixed with 10 mM EDTA for reaction termination. The radiolabeled products were then extracted with 1-butanol, and the radioactivities associated with aqueous and butanol phases were separately quantitated by using a

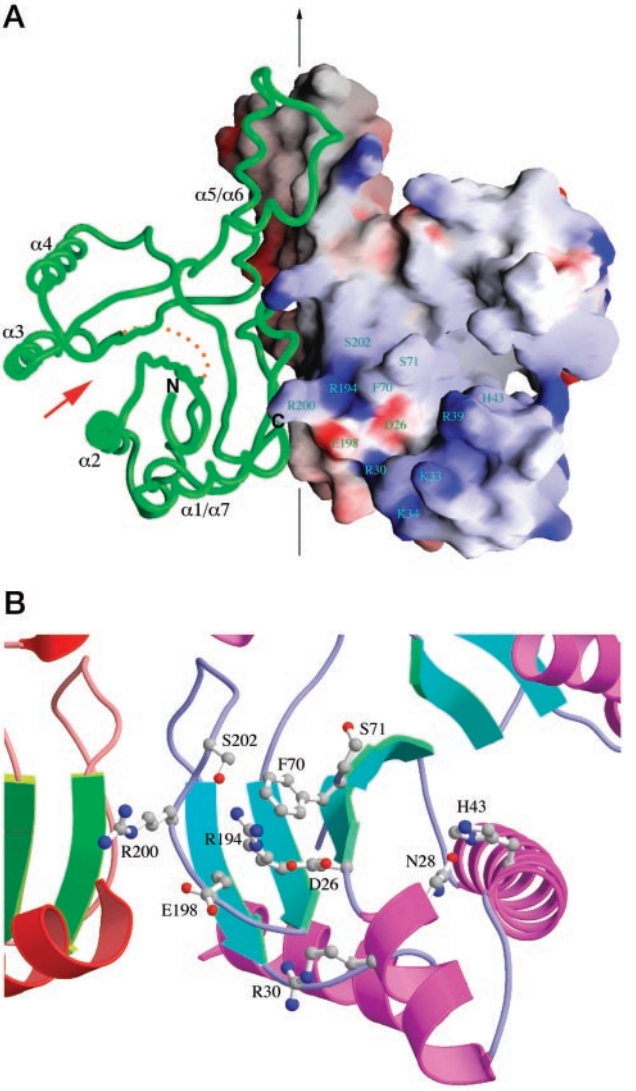

FIG. 2. *A*, GRASP representation (39) of the UPPs dimer with one subunit shown as "worm" tracing and another subunit as molecular surface with charge potential. The range is approximately −10 to 10 k_BT and coded *red* to *blue*. The unobserved loop is drawn as *orange spheres* in the *left subunit*. The *red arrow* indicates the location of the hydropobic tunnel, which is also seen in the *right subunit* as a hole in the surface. Several conserved residues in the vicinity of Asp-26, including Arg-30, His-43, Phe-70, Ser-71, Arg-194, Glu-198, Arg-200, and Ser-202, are labeled, as well as three additional positively charged residues Lys-33, Lys-34, and Arg-39. *B*, possible active site residues of UPPs. The *ribbon diagram* of the protein is viewed close-up in a direction similar to that of *A*, centered at the substrate-binding site. The side chains of nearby conserved residues, including the previous nine and Asn-28, are shown as *ball-and-stick* models. The figure is produced using MolScript and Raster3D (40).

Beckman LS6500 scintillation counter. Initial velocity data were fitted to Equation 1 to obtain K_m and k_{cat} values by non-linear regression (KaleidaGraph computer program). The k_{cat} was calculated from $V_{max}/[E]$.

$$v_0 = V_{max}\,[S]/(K_m + [S]) \qquad \text{(Eq. 1)}$$

where v_0 is the initial velocity; $[E]$ is the enzyme concentration; $[S]$ is the substrate concentration; V_{max} is the maximum velocity; and K_m is the Michaelis constant.

Product Formation and Analysis—The reaction rates of the wild-type and mutant enzymes I62A, H103A, L137A, and V105A were measured under the same conditions with 0.1 μM enzyme, 5 μM FPP, 50 μM [^{14}C]IPP, 0.5 mM $MgCl_2$, 50 mM KCl, and 0.1% Triton X-100 in 100 mM KOH-Hepes buffer, pH 7.5. Based on the reaction rate, the reaction mixture containing 0.5 μM mutant UPPs under the above reaction condition was incubated at 25 °C for 2 and 96 h in the presence and

absence of 0.1% Triton, respectively, to obtain the products. The reaction was then terminated with 10 mM EDTA, and the radiolabeled products were extracted with 1-butanol (IPP was in aqueous phase). After the removal of 1-butanol by evaporation, the 20% propanol solution containing 4.4 units/ml acid phosphatase, 0.1% Triton X-100, and 50 mM sodium acetate, pH 4.7, was used to convert polyprenyl pyrophosphate products to the corresponding polyprenols (35). The polyprenols were extracted with *n*-hexane, and the *n*-hexane volume was reduced by evaporation. The residual *n*-hexane solution was spotted on a reversed-phase TLC plate, which was then developed using acetone/water (19:1) as the mobile phase. The plate with radiolabeled products was analyzed by autoradiography using a bioimaging analyzer (Fujifilm BAS-1500). The products were identified by the R_f values reported previously (23). The percentages of the intermediates and product formed in the UPPs reaction were calculated from the measured intensities normalized by the numbers of [^{14}C]IPP incorporated.

Single Turnover Experiments of A69L and A143V—A rapid-quench apparatus (Kintek, Austin, TX) was employed to terminate the reactions catalyzed by A69L and A143V after a specified reaction time. For each reaction, 15 μl of enzyme solution, preincubated with FPP, were mixed with an equal volume of [^{14}C]IPP solution to start the reaction. The reaction solution contained 10 μM mutant enzyme, 2 μM FPP, 50 μM [^{14}C]IPP, 0.5 mM $MgCl_2$, 50 mM KCl, and 0.1% Triton in the buffer of 100 mM KOH-Hepes, pH 7.5, and 25 °C. The reaction was terminated by the addition of 67 μl of 0.6 N NaOH. It was demonstrated previously that 0.4 N (after mixing) base was able to stop the reaction immediately (23). Quenched reaction solutions were analyzed for intermediates and product by using the TLC method described above.

RESULTS AND DISCUSSION

Overall Structure—Each asymmetric unit of the crystal unit cell contains one UPPs dimer, which is the active form of the enzyme. The dimer has a peanut shape of 35 × 70 Å when viewing along the dyad axis direction. When the dimer is viewed perpendicular to the dyad axis, it has the shape of a butterfly (Fig. 1). Each subunit contains two domains, a catalytic domain (the butterfly wings) and a pairing domain (the butterfly body). The dimer has a novel global folding structure in which the two monomers are tightly associated via an extensive interface between the edges of the central β-sheet and between a pair of long α-helices (α5 and α6).

The catalytic domain adopts a parallel α/β topology that resembles the Rossmann fold. There are six parallel β-strands with the arrangement of a βC-βD-βB-βA-βE-βF topology. The six-stranded β-sheet adopts an incomplete cone shape with about 40% of the surface open. The C terminus lies on the pointed side with a hole of about 10 Å in diameter, where the putative active site is located (see below). The N-terminal end of the cone has a diameter of about 25 Å.

There are 7 α-helices, with α1(Gly-27 to Gly-36), α2 (Arg-39 to Asn-60), α3 (Ser-83 to His-103), α4 (Asn-117 to Gly-133), and α7 (Asp-225 to Glu-240) on the outer surface of the β-cone, and α5 and α6 fill the opening of the β-cone. Three 3_{10} helices connect between α5 and α6 (Gln-168 to Ile-172), βE and βF (Leu-206 to Ala-210), and βF and α7 (Leu-220 to Phe-224), respectively. All helices are mostly straight, except for α3, which is kinked. It is interesting to note that the location of the kink in α3 is different in the two subunits that may be relevant to the product release (see below). The conformations of the two subunits are nearly identical, except for the conformation and the relative disposition of helix α3.

Helices α5 and α6 and their associated turns are involved in the dimer formation with the major stabilization coming from the coiled-coil structure of the α5-α5 hydrophobic interactions. It is further enhanced by 24 hydrogen bonds involving 11 residues of one subunit, and their equivalents of the other subunit, plus 6 water molecules. The side chain of Arg-148 is stacked with that of Trp-207 from the other subunit.

The second region of the interface, constituted by strand βF, its proceeding turns, and the polypeptide C terminus, also involves hydrophobic interactions. The patch formed by the side chains of Ile-201, Leu-206, Ile-209, Ala-210, Leu-214, and Phe-216 extends the hydrophobic core of one subunit (on the concave side of the β-cone) across the molecular dyad to another subunit. There are 42 hydrogen bonds between the subunits.

Product and Substrate Binding Site—An intriguing question regarding the mechanism of UPPs is the exquisite ability of the enzyme to synthesize precisely a product containing 11 prenyl units (55-carbon). We have examined the three-dimensional structure of the enzyme to seek a clue to this question. We have found that there is an elongated tunnel within which the hydrophobic amino acids side chains cover the entire surface. Interestingly, this hydrophobic tunnel, surrounded by 4 β-strands (βA-βB-βD-βC) and 2 α-helices (α2 and α3), is not the same for the two subunits. In one subunit, the tunnel is narrow within which an elongated electron density envelope, suggestive of an aliphatic fragment, is clearly visible. In the other subunit, the tunnel is more open where only water molecules are found. Fig. 2*A* shows the surface drawing of the enzyme in which the more open subunit is oriented in such a way that the tunnel is clearly visible. On the top of tunnel, there are several conserved hydrophilic amino acids in the vicinity of Asp-26, including Asn-28, Arg-30, His-43, Phe-70, Ser-71, Arg-194, and Glu-198. Fig. 2*B* shows the detailed arrangement of these amino acids. This region has been suggested as the FPP- and IPP-binding site based on site-directed mutagenesis studies (24, 36).

We compared the two subunits by least squares superposition shown in Fig. 3*A*. In this diagram, we are looking into the tunnel from the side. Most of the backbones are superimposed very well, except for the two helices α3 and α4, with a r.m.s.d. of 2.7 and 1.5 Å, respectively. Here the *magenta* and *red* helices are associated with the "open tunnel" and "closed tunnel" forms of the two subunits, respectively. It is interesting to note that both α3 helices are kinked, but at different locations. The *magenta* helix is kinked by ~30° at Glu-96, and the *red* helix is kinked by ~45° at Ala-92.

The *red* helix is translocated upward by about one-half turn of α-helix (2.7 Å) and laterally toward α2 helix by 2.5 Å, making the inside space of the tunnel tighter and shorter. The resulting tight space allows a better binding of the hydrophobic aliphatic fragment such that it becomes visible in the electron density (Fig. 3*A*). This aliphatic fragment may be coming from either the Triton X-100 or PEG8000.

The detailed structure of the tunnel may be schematically illustrated using a cylindrical projection diagram in Fig. 3*B*. It can be seen that the interior of the tunnel is completely hydrophobic, except near Asp-26 of the *upper left corner* where the putative substrate-binding site is. The depth of the hydrophobic tunnel is ~30 Å, which is sufficient to accommodate the C_{55}-prenyl chain.

Comparison of UPPs Structures from E. coli and M. luteus—The structures of UPPs from *E. coli* and *M. luteus* are globally similar to each other, as evident in the root mean square deviation (r.m.s.d.) of 1.38 Å for 377 matched pairs of α-carbon atoms. The r.m.s.d. is 0.79 Å for 274 atom pairs when a matching criterion of 1.5 Å is used. The largest deviations are located in helices α3 and α4, which are relevant to the catalytic function of UPPs. As mentioned above, two conformations for the two subunits of *E. coli* UPPs dimer are observed. In contrast, the two subunits in *M. luteus* UPPs have identical structure that is similar to the closed form of *E. coli* UPPs. Compared with the closed form of *E. coli* UPPs, the α4 helix in one subunit of the *M. luteus* enzyme significantly differs by rotation of about 20° anchored on its C terminus, and the maximal displacement is ~6.5 Å at its N terminus, whereas α3 differs by

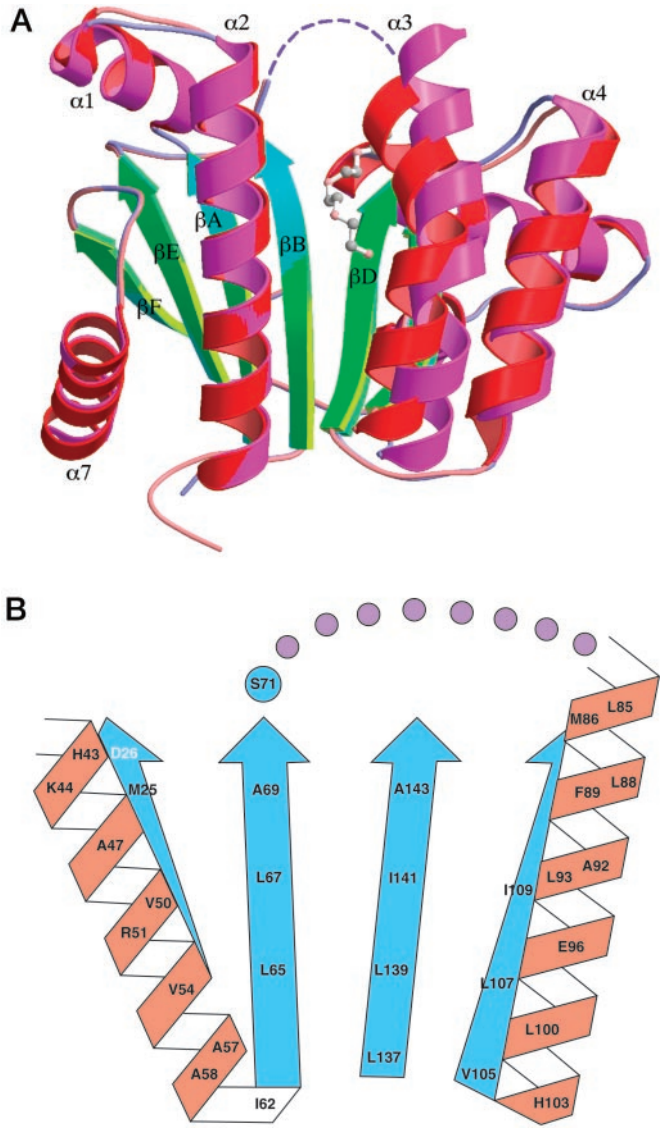

FIG. 3. **Hydrophobic tunnels of UPPs.** *A*, the two subunits, colored as in Fig. 1, are superimposed as described in the text. The ribbon drawing was produced using MolScript and Raster3D. The PEG fragment observed in subunit A is shown as *ball-and-stick* model. The loop between strand βD and helix α3 is shown as *dashed lines*. *B* is a schematic cylindrical projection diagram of the opened up tunnel. The two helices α2 and α3 are rotated such that residues facing the tunnel is visible. All of the labeled residues contribute to the wall of the tunnel, except Asp-26 on the opposite side of the β-strand.

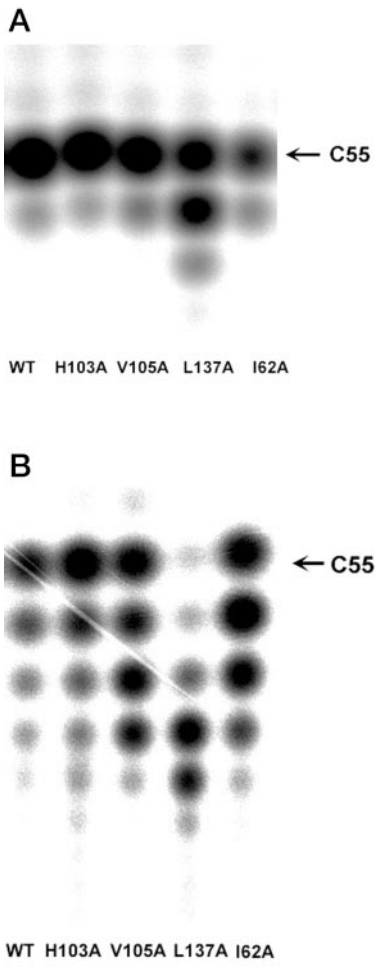

FIG. 4. **The products synthesized by I62A, L137A, V105A, and H103A in the presence of Triton (*A*) and in the absence of Triton (*B*).** The reaction mixture containing 0.5 μM each mutant enzyme, 5 μM FPP and 50 μM [^{14}C]IPP, was incubated at 25 °C for 2 h in the presence of Triton and 96 h in the absence of Triton to complete the reaction. The final products were extracted and analyzed using TLC and PhosphorImager. Lanes from *left* to *right* represent the products for the wild type, H103A, V105A, L137A, and I62A, respectively. The L137A catalyzes the formation of longer products compared with the wild-type UPPs under both conditions.

only about 2 Å. On the other hand, both of the entire helices α3 and α4 are moved by 5–7 Å in the other subunit, which show a manifestation of contrasting open and closed forms. In addition, helix α6 and the associated loops also show deviation of 1.5–3 Å in the two UPPs structures, possibly correlated with the open-closed conformational change. Because only the closed form was observed for *M. luteus* UPPs, Fujihashi *et al.* (25) reported a large cleft surrounded by the S2- and S4-strands and the H2 and H3 helices (equivalent to βB, βD, α2, and α3 in the terminology used in this paper). We observe the open form in which two additional β-strands (βA and βC) may also constitute the hydrophobic tunnel. These structural deviations might result from the different crystal packings or different conditions utilized in protein crystallization. Triton and PEG were included in crystallization of *E. coli* UPPs, whereas the heavy atom derivatives were contained in the soaking buffer of *M. luteus* enzyme.

Products Generated by I62A, H103A, V105A, and L137A UPPs—The structure of *E. coli* UPPs reveals a hydrophobic tunnel formed by 4 β-strands (βA-βB-βD-βC) and 2 helices (α2 and α3), sufficiently large to accommodate the entire UPP. Large amino acid residues, which include Ile-62, Leu-137, Val-105, and His-103, occupy the bottom portion of the tunnel (Fig. 3*B*). We proposed that one or more of these residues might play a role in determining product chain length, analogous to the above-mentioned amino acid residue located upstream from the first DD*XX*D motif in *E*-type prenyltransferases. To test this proposal, site-directed mutagenesis was performed to replace these large residues with Ala, and the chain lengths of the products synthesized by the mutant enzymes were examined by TLC analysis. The activities of H103A, V105A, L137A, and I62A mutants, assayed with 5 μM FPP and 50 μM [^{14}C]IPP, are within a 5-fold range of the wild-type UPPs activity. Reactions of 0.5 μM wild-type UPPs and 0.5 μM mutant UPPs, with 5 μM FPP and 50 μM [^{14}C]IPP for 2 h in the presence of 0.1% Triton X-100 and 96 h in the absence of Triton, lead to the formation of product mixtures shown in Fig. 4, *A* and *B*. Previous studies (23) have shown that Triton X-100 facilitates product release, and the UPPs reaction is fast in the presence of Triton. The

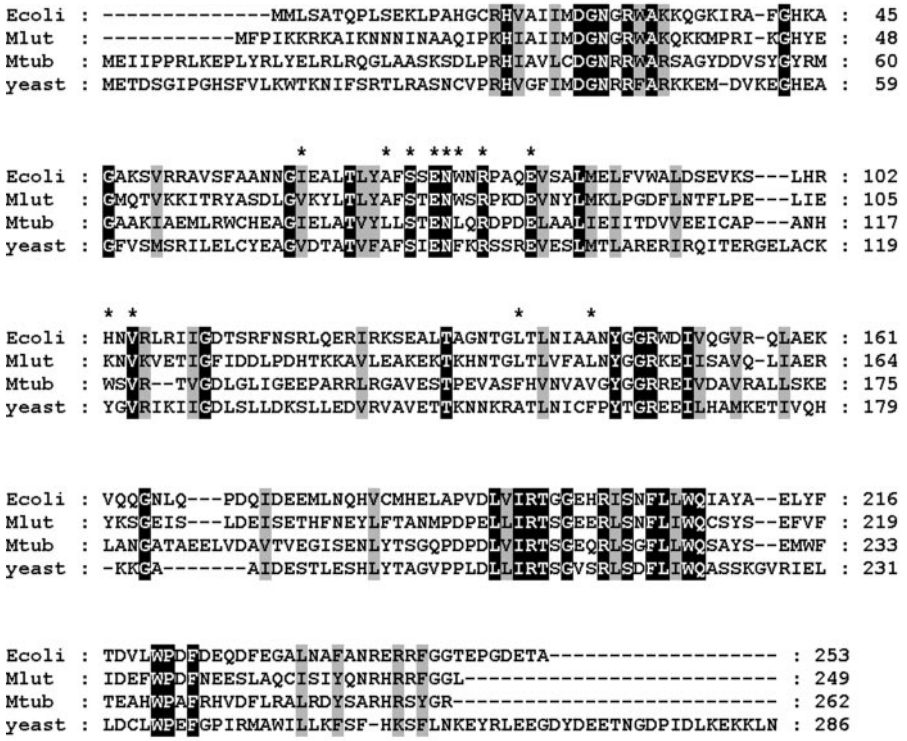

FIG. 5. **Alignment of amino acid sequences of the *E. coli* UPPs (Swiss-Prot Q47675), the *M. luteus* UPPs (GenBank™ AB004319), the *Z*-type farnesyl-pyrophosphate synthase Rv1086from *M. tuberculosis*, and the yeast dehydrodolichyl-pyrophosphate synthase RER2 (Swiss-Prot P35196) (*Mlut*, *M. luteus*; *Mtub*, *M. tuberculosis*).** *Black* and *gray outlines* indicate identical and similar amino acid residues, respectively. The *asterisks* indicate the amino acid residues mutated in this study. The amino acid residues corresponding to Ala-69 and Ala-143 of *E. coli* UPPs are Leu-84 and Val-156 in the *M. tuberculosis* FPPs and Ala-72 and Leu-146 in the *M. luteus* UPPs. Leu-137 in *E. coli* UPPs corresponds to Ala-154 in yeast RER2 protein.

major product for the wild-type UPPs-catalyzed reaction carried out in the presence of Triton is C_{55} (C_{55}:C_{60} = 96:4, *1st lane* of Fig. 4*A*). This is also the case for the H103A, V105A, and I62A UPPs-catalyzed reactions (*2nd, 3rd,* and *5th lanes* in Fig. 4*A*). L137A UPPs, on the other hand, promotes the synthesis of C_{55} and C_{60} polymers mainly and C_{65} to a lesser extent (C_{55}:C_{60}:C_{65} = 55:41:4, Fig. 4*A, lane 4*). Because of the slow product release that occurs in the absence of Triton (Fig. 4*B*), wild-type, H103A, V105A, and I62A UPPs cause the formation of C_{55}-C_{75} products with C_{55} as the major component. As calculated from the imaging intensity divided by the number of IPP incorporated in each product, wild-type and H103A show similar product distributions (C_{55}:C_{60}:C_{65}:C_{70}:C_{75} = 56:26:11:6:1, *1st lane* for wild-type enzyme and C_{55}:C_{60}:C_{65}:C_{70}:C_{75} = 54:25:12:7:2, *2nd lane* for H103A). V105A and I62A mutations result in higher ratios of C_{60} and C_{65} compared with that of the wild-type UPPs, and V105A synthesizes significant amount of C_{70} (C_{55}:C_{60}:C_{65}:C_{70}:C_{75} = 37:24:22:15:2, *3rd lane* for V105A; C_{55}:C_{60}:C_{65}:C_{70}:C_{75} = 35:33:21:9:2, *5th lane* for I62A enzyme). In contrast, L137A UPPs produces C_{70} and C_{75} as the major products (C_{55}:C_{60}:C_{65}:C_{70}:C_{75}:C_{80} = 3:5:17:40:29:5, Fig. 4*B, 4th lane*).

Based on these findings, we hypothesized that the substitution of the large side chain in Leu-137 with a smaller side chain in Ala removes the floor of the tunnel, thereby allowing for the formation of longer chain length products. Based on the crystal structure, the Ile-62 and His-103 side chains are directed away from the tunnel, and the side chains of Leu-137 and Val-105 are pointed toward the tunnel interior. Leu-137 is positioned on the same side of the α-1 helix used to bind FPP, whereas Val-105 is not. Apparently, Leu-137 is positioned to prevent further elongation of C_{55}. However, Val-105 may also play a role in determining product chain length because its mutations increase the ratios of C_{60}, C_{65}, and C_{70} but is not as critical as Leu-137. This conclusion is supported by the observation that dehydrodolichyl-pyrophosphate synthase from *Saccharomyces cerevisiae*, which catalyzes formation of longer chain length C_{70}-C_{80} products (37), has an Ala (Ala-154) at the position corresponding to Leu-137 in *E. coli* UPPs (see Fig. 5). Because of the presence of the small Ala residue, the chain elongation in the yeast enzyme does not stop at C_{55} but continues to generate longer chain products.

Intermediates of A69L and A143V UPPs-catalyzed Reactions Monitored under Single Turnover Conditions—An unusual *Z*-type FPPs, recently found in *M. tuberculosis* and shown to be homologous to UPPs in primary sequence, synthesizes a short chain rather than typical long chain polyprenyl pyrophosphate product (26). Two amino acid residues, Ala-69 and Ala-143, located near the top of the hydrophobic tunnel in *E. coli* UPPs, are replaced by Leu and Val, respectively, in the *M. tuberculosis Z*-type FPPs (Fig. 5). We hypothesize that Ala-69 or Ala-143 might be positioned near the FPP-binding site of UPPs about midway in FPP chain elongation to C_{55}. Replacement of these residues in UPPs with Leu and Val would, in analogy to the *M. tuberculosis* enzyme, limit the chain elongation and thus cause the formation of a short chain product. Site-directed mutagenesis methods were used to test this proposal. Upon extended incubation for 2 h in the presence of 0.1% Triton, the A69L mutant converts the substrate to mainly C_{50} product, whereas the A143V mutant generates the C_{55} product (data not shown). No evidence was found for the formation of short chain products in these reactions. However, when we examined the formation of intermediates, the impact of the amino acid substitutions on the elongation process became clear. For this analysis, the enzyme is used at high concentration (10 μM) with a limiting amount of substrate in order to maximize the relative quantities of intermediates formed. Under such conditions, the reaction proceeds rapidly, and therefore, it is carried out in a rapid-quench apparatus. This allows for termination of the enzyme-catalyzed reaction following short incubation periods.

As shown in Fig. 6*A*, the synthesis of C_{45} and C_{50} using the A69L mutant is complete in 15 s (extended reaction periods lead to the slow conversion of C_{45} to C_{50}, data not shown). Within the 15-s time frame, formation of C_{20}–C_{40} intermediates can be observed. In the wild-type UPPs reaction, intermediates are transiently formed and are disappearing, whereas

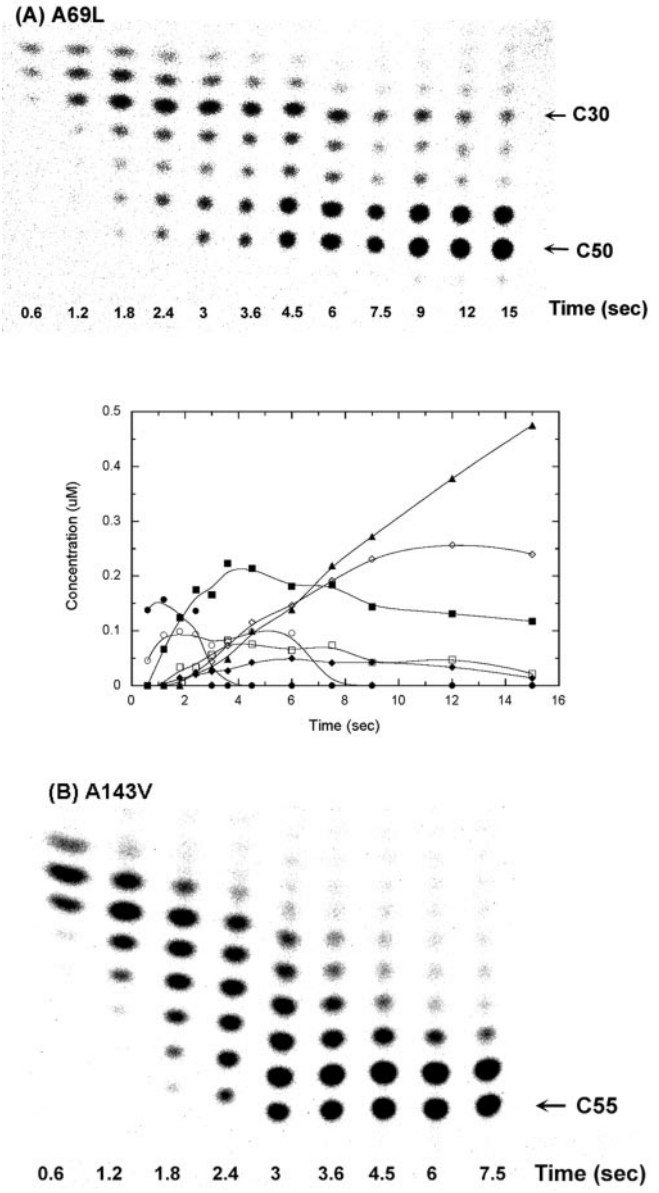

FIG. 6. **Single turnover experiments of A69L (*A*) and A143V (*B*) to examine the possibility of production of short chain intermediates.** In the reaction at 25 °C, 10 μM mutant enzyme, 2 μM FPP, and 50 μM [^{14}C]IPP were used. The reaction was terminated after a specified reaction time using rapid-quench instrument, and the intermediates formed at each time point were analyzed using TLC. A quantitative expression of the image data for A69L is also shown (C_{20} (●), C_{25} (○), C_{30} (■), C_{35} (□), C_{40} (♦), C_{45} (◇), and C_{50} (▲)). *A*, for the single turnover reaction of A69L, accumulations of C_{30} to a greater extent and longer times compared with the other intermediates were observed. Finally, A69L synthesized C_{50} as major product, whereas A143V produced C_{55}-UPP.

the next intermediate is gradually formed (23). In contrast, the C_{30} intermediate of A69L reaction accumulates to a greater extent (*e.g.* C_{20}:C_{25}:C_{30}:C_{35}:C_{40}:C_{45}:C_{50} = 0:14:27:9:7:22:21 for 6-s reaction) and lasts longer (C_{20}:C_{25}:C_{30}:C_{35}:C_{40}:C_{45}:C_{50} = 0:0:14:2.5:1.5:27:55 at the end of 15 s) than the other intermediates. The quantitative time course data of A69L reaction are shown on the bottom of Fig. 6*A*. The substitution of Ala-69 with Leu might also force a slight change of the direction of chain elongation leading to shorter product C_{50}. In contrast, the A143V-catalyzed reaction displays only the transiently formed intermediates similar to the wild-type UPPs but with 3-fold smaller rate constant for IPP condensation (Fig. 6*B*, quantitative data not shown). Based on the data, the Ala-69 but not Ala-143 is positioned in UPPs such that it does not affect the binding of intermediates shorter than C_{30} but interferes with proper binding of C_{30} and longer polymers.

It was proposed that the FPP site is probably located in the area of Asp-26, the *upper-left corner* of the tunnel shown in Fig. 3*B*. It is apparent from the crystal structure that Ala-69 is closer to the binding site of FPP, and Ala-143 is more distant from this site. In addition, Ala-69 in *E. coli* UPPs is conserved in *M. luteus* enzyme, but the corresponding residue of Ala-143 is a larger residue Leu in *M. luteus* UPPs (see Fig. 5). Our experimental data indicate that a small residue like Ala at position 69 but not 143 is required for continued chain elongation to C_{55} catalyzed by UPPs. The accumulation of C_{30} in the single turnover of A69L indicates that the space between Ala-69 and the FPP-binding site allows the incorporation of three IPP molecules. However, the mutation of Ala-69 to Leu does not completely block the chain elongation at this point (probably due to the large room of the hydrophobic tunnel), and the reaction continues to produce C_{45} and finally C_{50}. However, reversible release and temporary accumulation of the C_{30} intermediate occur with this mutant.

The Roles of Amino Acid Residues in the Disordered Loop of 72–83—The 72–83 loop is not visible in both x-ray crystal structures of UPPs (see Fig. 3*B*), and thus it is not possible to know what role, if any, these residues play in catalysis. Previous studies indicated that Asn-77 and Trp-78 in *M. luteus* UPPs (corresponding to Asn-74 and Trp-75 in *E. coli* enzyme) are important in catalysis and FPP binding. Substitution of Asn-77 with Ala, Asp, or Gln causes a 10^2–10^3-fold reduction in k_{cat}. Replacement of Trp-78 with Ile, Arg, or Asp increases the FPP K_m by ~5–20-fold (27). In the current study, we sequentially replaced the polar amino acid residues and Trp-75 of the loop of the *E. coli* enzyme with Ala and measured the kinetic properties of the mutant enzymes (Table II). S71A, N74A, and R77A UPPs show markedly decreased k_{cat} values. W75A and E81A UPPs as well as the previously characterized E73A UPPs (24) display smaller reductions in k_{cat}. The k_{cat} values for S71A, E73A, N74A, W75A, R77A, and E81A are 0.11, 0.3, 2.2×10^{-2}, 1.1, 1.4×10^{-4}, and 0.4 s^{-1}, respectively, whereas that of the wild-type enzyme is 2.5 s^{-1}. Consistent with the behavior of the corresponding *M. luteus* UPPs mutants (27), the N74A mutation in *E. coli* UPPs results in a 100-fold decrease of k_{cat} value with no increase in FPP and IPP K_m values. The substitution of Trp-75 with Ala increases the K_m values for FPP and IPP 8- and 11-fold, respectively, in *E. coli* UPPs reaction. E81A and S71A have significantly lower IPP affinities as indicated by their increased (22–33-fold) IPP K_m values.

These results indicate that the loop is responsible mainly for IPP binding, and Trp-75 is involved in FPP binding. As shown in Fig. 2*B*, Ser-71 (positioned at the end of the loop) together with Phe-70 are located in the substrate-binding site and may interact with IPP and place it in a correct position relative to FPP for the condensation reaction to occur. This hypothesis is supported by a recent report suggesting that Phe-73 and Ser-74 (equivalent to Phe-70 and Ser-71 in *E. coli* enzyme) are important for IPP binding and catalysis in *M. luteus* UPPs (36). In addition, our studies demonstrate that Glu-81 and some other amino acid residues in the loop, which are invisible in the crystal structure, are also critical in substrate binding and/or catalysis in *E. coli* UPPs.

Two protein conformers are observed in the *E. coli* UPPs structure. The major difference is that the α3 helix is kinked to a greater degree in the conformer that contains Triton or PEG (used in the crystallization solution). This conformer (closed form) has a tighter space, which allows for better binding of the hydrophobic aliphatic fragment. The other conformer (open

TABLE II
Kinetic parameters of mutant E. coli UPPs in the region of the flexible loop compared with the wild-type enzyme

UPPs	k_{cat}	K_m (FPP)	K_m (IPP)	relk_{cat}[a]
	s^{-1}	μM		
Wild type	2.5 ± 0.1	0.4 ± 0.1	4.1 ± 0.3	1
S71A	0.11 ± 0.01	1.0 ± 0.2	133 ± 14	4×10^{-2}
E73A[b]	0.30 ± 0.01	0.4 ± 0.1	16.2 ± 2.2	0.1
N74A	$(2.20 \pm 0.03) \times 10^{-2}$	0.4 ± 0.1	8 ± 0.6	1×10^{-2}
W75A	1.1 ± 0.1	3.2 ± 0.3	46 ± 4	0.5
R77A	$(1.4 \pm 0.1) \times 10^{-4}$	1.6 ± 0.3	15.7 ± 2.5	5×10^{-3}
E81A	0.4 ± 0.1	0.4 ± 0.1	88 ± 10	0.2

[a] k_{cat} relative to that of wild type.
[b] Data taken from Ref. 24.

form) only contains water in the substrate binding region. As shown in Fig. 3*B*, the α3 helix is linked to the flexible loop 71–83. IPP binding might trigger the movement of the loop toward the substrate-binding region of Asp-26, and this might induce a conformational change from the open form to the closed form that results in enhanced interactions of enzyme with substrate. After UPP is formed, the closed form can switch back to the open form to release the product. The loop might be utilized as a hinge for the interconversion of two conformers and as a control mechanism for substrate binding and product release.

Conclusions—The *E. coli* UPPs structure reported here is consistent with that of the *M. luteus* UPPs. However, compared with the *M. luteus* UPPs structure, our *E. coli* enzyme structure has a better resolution (1.8 *versus* 2.2 Å) and provides more detail in structural information. Furthermore, two enzyme conformers of *E. coli* UPPs are identified, which may be related to a gate opening/closing mechanism for the release of the product. The site-directed mutagenesis studies reported in this paper provide further insight into the catalytic mechanism of UPPs by identifying the following: (i) important amino acid residues that determine the product chain length, and (ii) the functions of amino acid residues located on the flexible active site loop. We conclude that the bulky side chain of Leu-137 serves to block further elongation of UPP based on the finding that substitution of Leu-137 with Ala results in the synthesis of longer polyprenyl products. The Ala-69 amino acid is located at a distance corresponding to three isoprene units away from FPP bound in *E. coli* UPPs. The substitution of Ala-69 with Leu results in long lived accumulation of a short chain intermediate C_{30}. Thus, the elongation process needed for formation of the correct C_{55} product in wild-type UPPs is regulated by the small size of the Ala residue located at position 69 and the large size of the Leu resided at position 137.

The amino acid residues of the flexible loop are important for catalysis as well as substrate binding, particularly IPP binding. The flexibility of the UPPs structure and the involvement of several residues in IPP binding are required because the enzyme catalyzes multiple IPP condensations leading to a large and highly hydrophobic product which must exit the active site.

The site-directed mutagenesis studies presented here along with the previously reported data provide a model (see Fig. 7) for UPPs catalysis and substrate binding that can be used to design studies, while the determination of the crystal structure of the enzyme substrate complexes is in progress. In addition to the hypothetical FPP and IPP binding mode reported by Fujihashi *et al.* (25), we provide information on the amino acid residues involved in the product chain length determination and the role of a flexible loop in the model. According to this model, FPP is bound with its PP_i group near the Asp-26, Asn-28, Arg-30, and Glu-198 area, likely with the help of Mg^{2+} ion(s). The C_{15}-farnesyl chain is bound with its tail pointing toward the bottom of the tunnel. The tunnel at this stage is

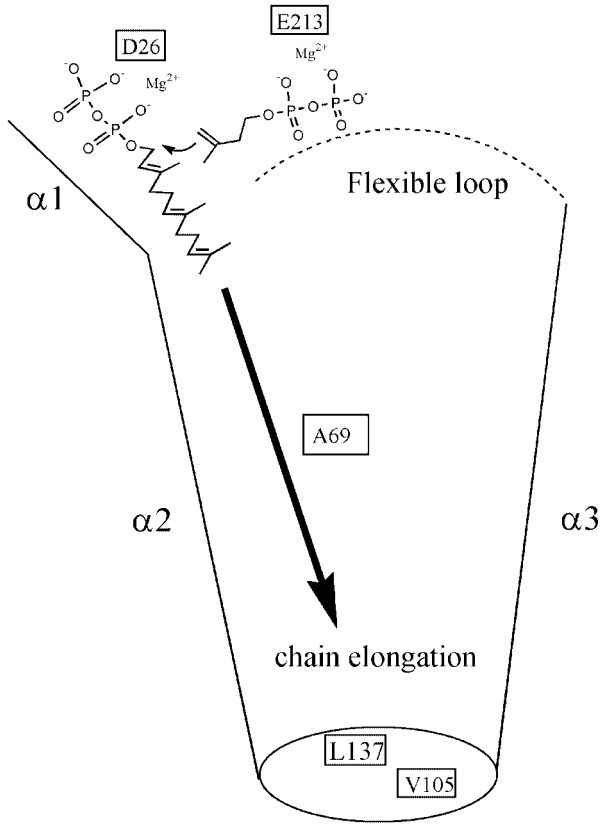

FIG. 7. **A model of UPPs catalysis and substrate binding.** As described in the text, FPP and IPP are bound near Asp-26 and Glu-213 in the region located on the top of the hydrophobic tunnel. FPP undergoes chain elongation by condensation with IPP and reaches the chain length of C_{55}. The Leu-137 is at the most critical position to block the further elongation of the product.

probably in the closed form, and the 71–83 loop is open and flexible. An incoming IPP (possibly assisted by the loop of residues 71–83) attacks the carbocation formed from the bound FPP. After the reaction, the free PP_i leaves and the pyrophosphate moiety of the C_{20}-compound is translocated to the Asp-26 site, ready for the next cycle. The extended C_{30} oligoprenyl chain passes by Ala-69 and condenses with five additional IPP units until the final product reaches Leu-137 located on the bottom of the tunnel. When the chain length reaches C_{55}, the dimethyl end is stopped at the end of the tunnel where the opening is small. At this point, the crowding between the prenyl chain and the 71–83 loop at the top of the tunnel forces the α3 helix to move away from the closed position into the open position. The fully synthesized C_{55}-PP product can exit easily from the open gate, especially in the presence of Triton or membrane lipid bilayer.

Acknowledgments—We thank J. J. Pan for assistance in preparing seleno-Met UPPs. We thank National Synchrotron Light Source for the use of synchrotron data collection.

REFERENCES

1. Ogura, K., Koyama, T., and Sagami, H. (1997) *Subcell. Biochem.* **28,** 57–88
2. Grunler, J., Ericsson, J., and Dallner, G. (1994) *Biochim. Biophys. Acta* **1212,** 259–277
3. Ogura, K., and Koyama, T. (1998) *Chem. Rev.* **98,** 1263–1276
4. Ogura, K., and Koyama, T. (1997) in *Dynamic Aspect of Natural Products Chemistry: Molecular Biology Approaches* (Ogura, K., and Sankawa, U., eds) pp. 1–23, Kodansha Ltd., Tokyo
5. Ashby, M. N., and Edward, P. A. (1990) *J. Biol. Chem.* **265,** 13157–13164
6. Koyama, T., Obata, S., Osabe, M., Takeshita, A., Yokoyama, K., Uchida, M., Nishino, T., and Ogura, K. (1993) *J. Biochem.* (*Tokyo*) **113,** 355–363
7. Chen, A., Kroon, P. A., and Poulter, C. D. (1994) *Protein Sci.* **3,** 600–607
8. Tarshis, L. C., Yan, M., Poulter, C. D., and Sacchettini, J. C. (1994) *Biochemistry* **33,** 10871–10877
9. Joly, A., and Edwards, P. A. (1993) *J. Biol. Chem.* **268,** 26983–26989
10. Song, L., and Poulter, C. D. (1994) *Proc. Natl. Acad. Sci. U. S. A.* **91,** 3044–3048
11. Koyama, T., Tajima, M., Nishino, T., and Ogura, K. (1995) *Biochem. Biophys. Res. Commun.* **212,** 681–686
12. Koyama, T., Tajima, M., Sano, H., Doi, T., Koike-Takeshita, A., Obata, S., Nishino, T., and Ogura, K. (1996) *Biochemistry* **35,** 9533–9538
13. Ohnuma, S., Suzuki, M., and Nishino, T. (1994) *J. Biol. Chem.* **268,** 14792–14797
14. Ohnuma, S., Hirooka, K., Hemmi, H., Ishida, C., Ohto, C., and Nishino, T. (1996) *J. Biol. Chem.* **271,** 18831–18837
15. Ohnuma, S., Hirooka, K., Naoki, T., Yano, M., Ohto, C., Nakane, H., and Nishino, T. (1998) *J. Biol. Chem.* **273,** 26705–26713
16. Tarshis, L. C., Proteau, P. J., Kellogg, B. A., Sacchettini, J. C., and Poulter, C. D. (1996) *Proc. Natl. Acad. Sci. U. S. A.* **93,** 15018–15023
17. Quellhorst, G. J., Jr., Piotrowski, J. S., Steffen, S. E., and Krag, S. S. (1998) *Biochem. Biophys. Res. Commun.* **244,** 546–550
18. Rip, J. W., Rupar, C. A., Ravi, K., and Carroll, K. K. (1985) *Prog. Lipid Res.* **24,** 269–309
19. Allen, C. M. (1985) *Methods Enzymol.* **110,** 281–299
20. Robyt, J. F. (1998) *Essentials of Carbohydrate Chemistry,* pp. 305–318, Springer-Verlag Inc., New York
21. Shimizu, N., Koyama, T., and Ogura, K. (1998) *J. Biol. Chem.* **273,** 19476–19481
22. Apfel, C. M., Takacs, B., Fountoulakis, M., Stieger, M., and Keck, W. (1999) *J. Bacteriol.* **181,** 483–492
23. Pan, J. J., Chiou, S. T., and Liang, P. H. (2000) *Biochemistry* **39,** 10936–10942
24. Pan, J. J., Yang, L. W., and Liang, P. H. (2000) *Biochemistry* **39,** 13856–13861
25. Fujihashi, M., Zhang, Y.-W., Higuchi, Y., Li, X.-Y., Koyama, T., and Miki, K. (2001) *Proc. Natl. Acad. Sci. U. S. A.* **98,** 4337–4342
26. Schulbach, M. C., Brennan, P. J., and Crick, D. C. (2000) *J. Biol. Chem.* **275,** 22876–22881
27. Fujikura, K., Zhang, Y.-W., Yoshizki, T., and Koyama, T. (2000) *J. Biochem.* (*Tokyo*) **128,** 917–922
28. Hendrickson, W. A., Horton, J., and LeMaster D. M. (1990) *EMBO J.* **9,** 1665–1672
29. Terwilliger, T. C., and Berendzen, J. (1999) *Acta Crystallogr. Sect. D Biol. Crystallogr.* **55,** 849–861
30. Terwilliger, T. C. (2000) *Acta Crystallogr. Sect. D Biol. Crystallogr.* **56,** 965–972
31. Collaborative Computational Project Number 4 (1994) *Acta Crystallogr. Sect. D Biol. Crystallogr.* **50,** 760–763
32. Perrakis, A., Sixma, T. K., Wilson, K. S., and Lamzin, V. S. (1997) *Acta Crystallogr. Sect. D Biol. Crystallogr.* **53,** 448–455
33. Jones, T. A., Zou, J. Y., Cowan, S. W., and Kjeldgaard, M. (1990) *Acta Crystallogr. Sect. A* **47,** 110–119
34. Brunger, A. T., Adams, P. D., Clore, G. M., Delano, W. L., Gros, P., Grosse-Kunstleve, R. W., Jiang, J. S., Kuszewski, J., Nilges, M., Pannu, N. S., Read, R. J., Rice, L. M., Simonson, T., and Warren, G. L. (1998) *Acta Crystallogr. Sect. D Biol. Crystallogr.* **54,** 905–921
35. Fujii, H., Koyama, T., and Ogura, K. (1982) *Biochim. Biophys. Acta* **712,** 716–718
36. Kharel, Y., Zhang, Y.-W., Fujihashi, M., Miki, K., and Koyama, T. (2001) *J. Biol. Chem.* **276,** 28459–28464
37. Bukhtiyarov, Y. E., Shabalin, Y. A., and Kulaev, I. S. (1993) *J. Biochem.* (*Tokyo*) **113,** 721–728
38. Kraulis, P. J. (1991) *J. Appl. Crystallogr.* **24,** 946–950
39. Nicholls, A., Sharp, K. A., and Honig, B. (1991) *Proteins* **11,** 281–296
40. Merrit, E. A., and Murphy, M. E. P. (1994) *Acta Crystallogr. Sect. D Biol. Crystallogr.* **50,** 869–873